Superpixel guided active contour segmentation of retinal layers in OCT volumes

Fangliang Bai, Stuart J. Gibson, Manuel J. Marques, Adrian Podoleanu

Fangliang Bai, Stuart J. Gibson, Manuel J. Marques, Adrian Podoleanu , "Superpixel guided active contour segmentation of retinal layers in OCT volumes," Proc. SPIE 10591, 2nd Canterbury Conference on OCT with Emphasis on Broadband Optical Sources, 1059106 (5 March 2018); doi: 10.1117/12.2282326

SPIE.

Event: Second Canterbury Conference on Optical Coherence Tomography, 2017, Canterbury, United Kingdom

Superpixel guided active contour segmentation of retinal layers in OCT volumes

Fangliang Bai, Stuart J. Gibson, Manuel J. Marques, and Adrian Podoleanu

University of Kent, Canterbury CT2 7NZ, Canterbury, UK

ABSTRACT

Retinal OCT image segmentation is a precursor to subsequent medical diagnosis by a clinician or machine learning algorithm. In the last decade, many algorithms have been proposed to detect retinal layer boundaries and simplify the image representation. Inspired by the recent success of superpixel methods for pre-processing natural images, we present a novel framework for segmentation of retinal layers in OCT volume data. In our framework, the region of interest (e.g. the fovea) is located using an adaptive-curve method. The cell layer boundaries are then robustly detected firstly using 1D superpixels, applied to A-scans, and then fitting active contours in B-scan images. Thereafter the 3D cell layer surfaces are efficiently segmented from the volume data. The framework was tested on healthy eye data and we show that it is capable of segmenting up to 12 layers. The experimental results imply the effectiveness of proposed method and indicate its robustness to low image resolution and intrinsic speckle noise.

Keywords: Optical coherence tomography, superpixel, active contour, retina segmentation, 3D model, retinal thickness

1. INTRODUCTION

Retinal OCT imaging is a very popular research topic and much effort has been devoted to improving the resolution and speed of OCT systems. In recent decades, optical coherence tomography has become an established technology for imaging the internal structures of the eye. Retinal OCT images are an important tool in ophthalmic disease diagnosis.[1] The morphological characteristics of retinal layers and the thickness of the individual layers have become important biomarkers for retinopathy in clinical diagnosis.[2]

In ophthalmic OCT, the presence of retinal tissue is determined by reflected light. The absorption and scattering between retinal tissue and embedded blood vessel (or its shadow) is inconsistent, which introduces challenge to accurate segmentation of the retinal layers. Furthermore, due to the nature of OCT systems, imaging quality is always affected by speckle noise and sometimes by additional image artifacts[3] caused by the acquisition process. To illustrate the aim of our work, Figure1 shows an annotated (ground truth) healthy retinal structure and Figure 2 shows two examples of OCT B-scans that are representative of the data used to test our method and for which we wish to detect the cell layers. The detection of layer boundaries is made difficult by speckle noise and inconsistent light reflection, present in Figure2 where the surface cell layer is brighter on the right hand side of the fovea.

The development of OCT retinal segmentation methods have been well documented in the last two decades since its early application in ophthalmology. A summary of these methods has been presented previously.[4] Existing approaches can be categorized into three groups: A-scan methods,[5,6,7] B-scan methods,[8,9,10,11] and 3D data based approaches.[12,13,14,15] A-scan based methods use the prior knowledge of the retinal structure to determine the location of different layers. The prominent layers in OCT retinal images are vitreous/NFL layer and RPE layer that exhibit strong reflection compared to neighboring layers. However, th e boundaries of other layers in A-scans can be difficult to determine due to the similarity of reflection from neighboring tissues. These methods are efficient to detect the prominent boundaries. However, they lack accuracy and robustness

Further author information: (Send correspondence to Fangliang Bai)
Fangliang Bai: E-mail: F.Bai@kent.ac.uk
Stuart J. Gibson: E-mail: S.J.Gibson@kent.ac.uk, Telephone: +44 01227 (82)3271

2nd Canterbury Conference on OCT with Emphasis on Broadband Optical Sources,
edited by Adrian Podoleanu, Ole Bang, Proc. of SPIE Vol. 10591, 1059106
 · doi: 10.1117/12.2282326

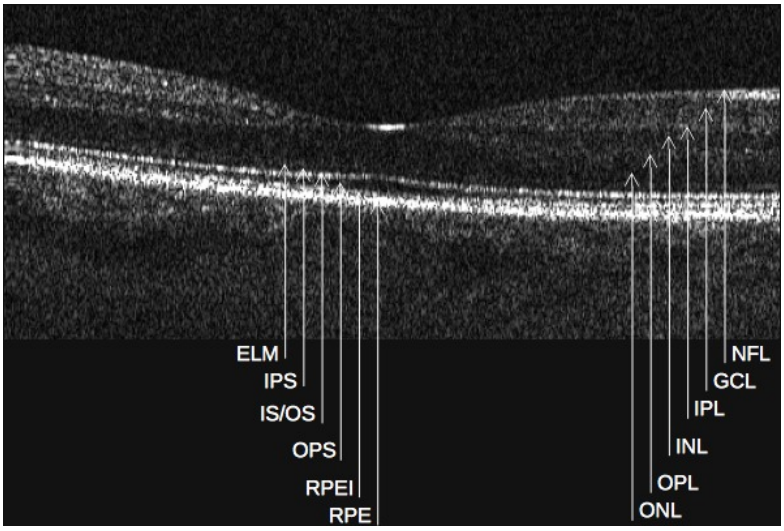

Figure 1. The annotation of healthy retina in OCT image. The B-scan image is scanned through the macula of a human retina. The annotated layers: Nerve Fiber Layer (NFL), Ganglion Ceil Layer (GCL), Inner Plexiform Layer (IPL), Inner Nuclear Layer (INL), Outer Plexiform Layer (OPL), Outer Nuclear Layer (ONL), External Limiting Membrane (ELM), Inner Photoreceptor Segm (IPS), Inner/Outer Photoreceptor Segm. (IS/OS), Outer Photoreceptor Segm. (OPS), Retinal Pigment Epithelium Interdigitation (RPEI), and Retinal Pigment Epithelium (RPE). The layers listed at left are discrete due to the fovea. The thin layers at bottom always have high light reflection while layers at top have high light absorption.

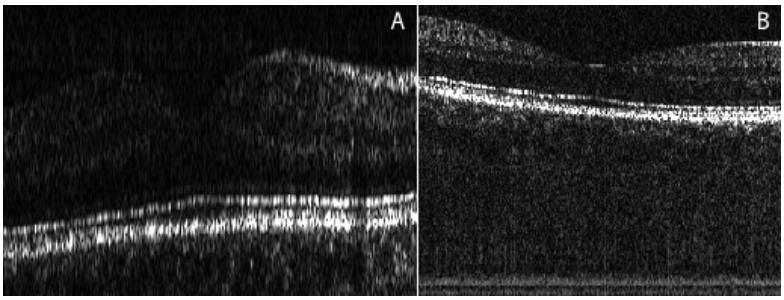

Figure 2. Two B-scan images used in the experiment. These images are generated from different OCT systems. (A): In the image, the contrast of retinal tissue is relatively low. (B): the retinal content has a relatively higher contrast. The stripe noise can be seen at the bottom of the image.

due to their susceptibility to speckle noise. A typical B-scan based approach is to build a mathematical model based on image gradient and other spatial information. Chiu *et al.*[8] represent the B-scan image as a graph and use graph-cut theory to find the path of lowest image energy, corresponding to the layer boundary. B-scan approaches are more accurate and stable than those based on A-scan images but are also affected by a lesser degree by speckle noise. Cell layer segmentation methods using 3D data require fast scanning speeds and large data storage capacity. Due to spontaneous movement of the eye, the 2D frames (B-scans) from which 3D volume data are constructed, have to be carefully registered. In addition, the large amount of B-scans in 3D data also limits the time efficiency of 3D data based approaches.

In this paper, we propose a novel cell layer segmentation method based on superpixels and active contours and applied to OCT data. Superpixel segmentation has attracted a lot of interest in medical imaging.[16] The segmentation of superpixels is realized based on local similarity of image content and spatial information. In our method, we determine 1D superpixels in A-scan images which corresponding to separate layers. Since the local reflection of retinal tissue are more consistent compared to that over entire layer, the similarity of local image content allows pixels to be grouped without being affected by pixels from other regions. The active contour has been widely used for object localization and edge detection in MRI and CT image processing.[17] The mathematical model for active contours is formed by an energy function. Updating the contour position is achieved by minimizing the energy function to a local minimum. In our work, we use an active contour to refine the segmentation with gradient and spatial information in the B-scan image. This corrects inconsistencies in A-scan segmentation using information present in the B-scan.

2. METHOD

The proposed framework consists of three parts, divided into two stages (localization and detection). In the first stage, the retinal region in a B-scan image is determined by an adaptive-curve boundary detection method. For the second stage, we represent the 1D A-scan data in terms of superpixels then use a modified active contour scheme to detect and refine the boundaries within the retinal region. Finally, an efficient volume segmentation is performed based on structural similarity of adjacent B-scans. This section describes each step in detail and then explains the overall framework.

2.1 Adaptive-curve Boundary Detection

We initialize the cell layer detection using an adaptive-curve boundary method to search for the retinal region of interest. In the B-scan image, the method selects a number of A-scans (usually less than 5) that are separated by equal distance intervals in the B-scan direction. In each individual A-scan, we search for the onset of the retinal region from two directions in A-scan data using a pixel intensity threshold. Since the high intensity contrast of NFL layer and RPE layer against to non-retinal region, the applied threshold is calculated by equation 1

$$D_{boundary} = \frac{1}{N}\sum_{i=1}^{N} x_i + \beta\sigma(x_{i,}), \quad i \in [1, ..., N] \tag{1}$$

Where N is number of rows from the top edge of B-scan image, where the vitreous has negligible intensity response, and σ is the standard variation of the all the pixels in N rows from the top of a B-scan and β is scaler defined by the user that controls the sensitivity of layer detection and must be adjusted according to the strength of the speckle noise. After the onset detection in selected A-scans, the boundary is estimated by interpolating a boundary line with B-splines. Based on curvature information of the initial boundary interpolation, the method re-samples A-scans (now at unequal spatial separations) thereby iteratively refining the boundary shape. This refinement process is achieved using an adaptive-curve algorithm that increases sampling density in regions of high curvature on the estimated boundary that are embedded in the B-scan images. The process is iterated until adjustment of the A-scan positions results in a boundary shape change that is equal to, or less than, the predetermined tolerance. The iterative boundary-updating process of vitreous/NFL boundary is shown in Figure 3 where the first boundary estimation is less accurate due to limited number of A-scans, while the updating process automatically corrects the boundary estimation with the adaptive-curve re-sampling scheme. After the determination of retinal region in B-scan image, we replace the non-retinal content with zeros and only focus on the retinal layers within the region.

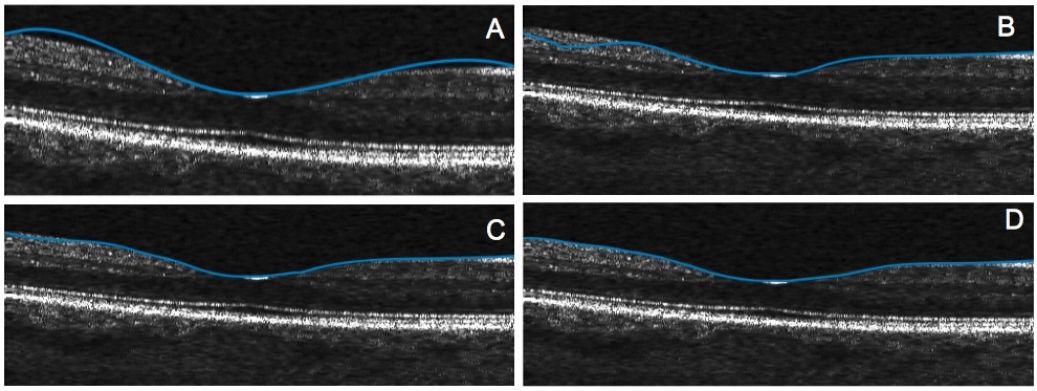

Figure 3. The segmentation of vitreous/NFL boundary by adaptive-curve detection method. Four figures shows the process of iterative boundary updating. (A): The initial interpolation with 5 A-scans detected. The approximated boundary is partially deviated from the actual position. (B-C): The adaptive-curve algorithm re-sampled the A-scan 4 times to updating the interpolated line. (D): The final results of boundary detection. The approximated line is fitted to the actual boundary shape.

2.2 Superpixel Segmentation

In the second stage, we first apply superpixels to determine the local region of internal layers. Superpixel segmentation is designed to generate a coherent grouping of pixels that contain similar grayscale and spatial information. In our work, we use the SLIC (Simple Linear Iterative Clustering) algorithm to segment internal layer boundaries since it produces superpixels at a low computational cost while achieving accurate segmentation.[18] Unlike previous applications of SLIC, that operate on 2D images, here we detect 'superpixels' in each 1D A-scan image within the region bounded by the top and bottom layers. In the SLIC algorithm, we first initialize a number of superpixels (and hence the number of layers) we wish to detect. Then, the SLIC method calculates the distance (similarity) of the seed, center pixel of the corresponding superpixel, and the neighboring unlabeled pixels using equation 2.

$$\begin{aligned} d_{lab} &= \sqrt{(l_k - l_i)^2} \\ d_x &= \sqrt{(x_k - x_i)^2} \\ D_s &= d_{lab} + \frac{m}{S} d_{xy} \end{aligned} \tag{2}$$

Where D_s is the sum of grayscale distance d_{lab} in Lab color space and spatial distance d_x in B-scan image. S is initial seed interval used for normalization and m is a variable controlling the balance of the two distance terms. This pixel labeling process is repeated for each seed and the resulting superpixels are formed. After the calculation for all superpixels, the algorithm updates the seeds (the spatial center of the superpixel). This updating iteration is terminated once the overall change of seeds position is less than a predetermined threshold, which indicates that the superpixels have become stable. Subsequently the shape of the cell layer is approximated by connecting corresponding boundaries between superpixels in adjacent A-scans. Figure 4 shows the segmented results of RPEI/RPE layer. In the limited search region, the algorithm generated two superpixels that form an approximated boundary, separating two slim layers in the narrow region. It can be observed that the approximation of the target boundary is not smooth and continuous. However, the superpixels perform consistently in both normal regions and others affected by the shadows of blood vessels. In addition, one should note that the A-scans close to the fovea contain fewer layers than other bilateral regions causing some A-scans to be over segmented. To counter this problem, we applied lateral limits after the segmentation of each layer boundary to restrict the search area. This is described in section 2.5.

2.3 Active Contour Boundary Detection

The initial, approximate, segmentation result achieved by the superpixel method is followed by a refining scheme implemented by the active contour. In this stage, we use a gradient-guided active contour. The active contour is

Figure 4. The segmentation results of RPEI/RPE boundary using superpixel algorithm. In the limited search area, Two superpixels separate the image content within A-scan, the formed boundary in B-scan image is not smooth and continuous, therefore cannot be accurately fitted to the actual position.

initialized after the superpixel stage and can be adapted to fit the boundary position by progressively minimizing an energy function[19] in equation 3.

$$E_{snake} = \int_0^1 (E_{internal}(v(s)) + \alpha E_{external}(v(s))) \tag{3}$$

$$E_{internal} = E_{cont} + E_{curv}$$

Where the energy function E_{scnake} contains an internal energy term $E_{internal}$ and an external energy (image gradient) term $E_{external}$. $v(s)$ represents all points on the contour and α is the sign for $E_{external}$. The internal term calculates bending rate E_{curv} and connectivity E_{cont} of the contour, while the external term controls the contour's adherence to layer boundaries. The boundaries are characterized by rapid changes in image intensity, either dim-to-bright or bright-to-dim. As a result, we specify a negative sign of E_{curv} in the energy function for dim-to-bright boundaries and positive sign for bright-to-dim boundaries. For example, the sign is positive for the IPL/INL boundary and negative for the INL/OPL boundary. This helps the active contour to reliably detect very closely separated boundaries. During the contour minimization, we constrain the update procedure for the active contour such that each control point (pixel in the contour) can only move in vertical steps of one pixel per iteration to enforce the connectivity as the retinal layer is continuous. This small step size is also appropriate for segmenting thin layer boundaries. The segmentation results for our active contour and the superpixel steps can be seen in Figure 5. It is clearly seen that the active contour method smooths the boundary between cell layers whereas the superpixel method alone does not. Hence the active contour corrects for local errors in boundary estimation.

2.4 Segmentation in Adjacent B-scans

After the second stage of proposed framework, one can segment boundaries in single B-scan image. We can also further segment the cell layers as surfaces in 3D volume from the B-scan segmentation. To implement the volume segmentation, we assume that the retinal structure in adjacent B-scan image changes gradually while remains similar to each other. We first segment boundaries with superpixels and active contours in a B-scan image, selected from either end of 3D volume. Then we use the segmented result as a predictor for the position of the same boundary in the adjacent B-scan image and then use an active contour to refine the position. Due to the spontaneous movement of eye or head, the resulting B-scans are poorly registered in the 3D volume representing the retina structure. To counter this problem, we select one B-scan from either end of the volume as a reference frame, to which other frames are registered. The registration process therefore enforces the smoothness of a layer surface within a 3D volume.

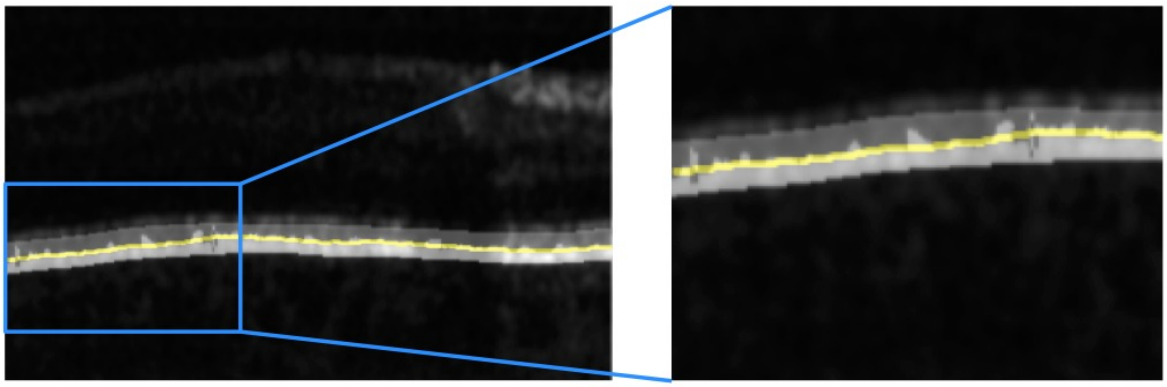

Figure 5. The refining results of active contour at RPEI/RPE boundary. The B-scan image is overlapped by the segmentation results by superpixel and active contour. Seen the zoomed window, the error generated by superpixel is corrected by active contour that results in a smooth and continuous line fitting well to the actual boundary shape.

2.5 Detection Sequence of Retinal Layers

We have thus far described a framework comprising three algorithms to segment a single retinal boundary in a single B-scan image or a 3D volume. In this section, we outline a sequential method for efficiently detecting multiple cell layers based on prior knowledge of the relative positions of these layers in retinal structures, taking into account the differences in tissue reflectivity.

2.5.1 Segmentation of low curvature layers

The retinal layers located at the bottom have higher intensity response and have simple and relatively flat structure, compared to upper layers. We begin by locating the salient (higher intensity response) IS/OS boundary and then use this as reference to identify the layers below it. The IS/OS layers are segmented by initializing two superpixels corresponding to top and bottom regions, followed by active contour with positive external term to smooth (denoise) the boundary. Next, we limit the search region from IS/OS to RPE and initialize superpixels for the remaining layers. After the superpixel segmentation, we select only one boundary from the top of the limited search region to which we apply an active contour. With this scheme, we can segment cell layers by gradually narrowing the search region in the order from top to bottom.

2.5.2 Segmentation of layers with varying curvature

The structure of the region above IS/OS changes through the foveal region. In general for OCT images scanned through the fovea, the intra-layers merge into fovea from side to center. While in other B-scans, the layers are stacked in the A-scan direction with each layer being approximately linear and horizontal. We use the IS/OS boundary as a reference for detecting OPL/ONL and apply the active contour with negative external term to correct the fit. This procedure is repeated for the remaining layers, located in the region limited by the vitreous/NFL (top) boundary and OPL/ONL (bottom) boundary. The remaining boundaries which are closer to the region edge (top and bottom boundaries) are segmented first, followed by those located in inner region with the IPL/INL being the last boundary to segment.

The boundary segmentation sequence is summarized in Figure 6. In the figure, a 10 layer segmentation is illustrated. However, it is possible to segment more layers using our method when the image quality is better. By increasing the number of superpixels extremely thin layers can be detected.

3. RESULTS AND DISCUSSION

We tested our method using OCT data provided by the Applied Optics Group University of Kent. The data was collected from two different OCT imaging systems. The data contains OCT volumes of the fovea regions from the healthy eyes of two volunteers. Each volume contains 192 frames (B-scans). The size of B-scan is 500×500. One of the volumes was denoised with a 3D median filter so that the performance of the method in the presence of noise could be assessed. Each volume was registered by StackReg in ImageJ. The framework was implemented using MATLAB in a general PC.

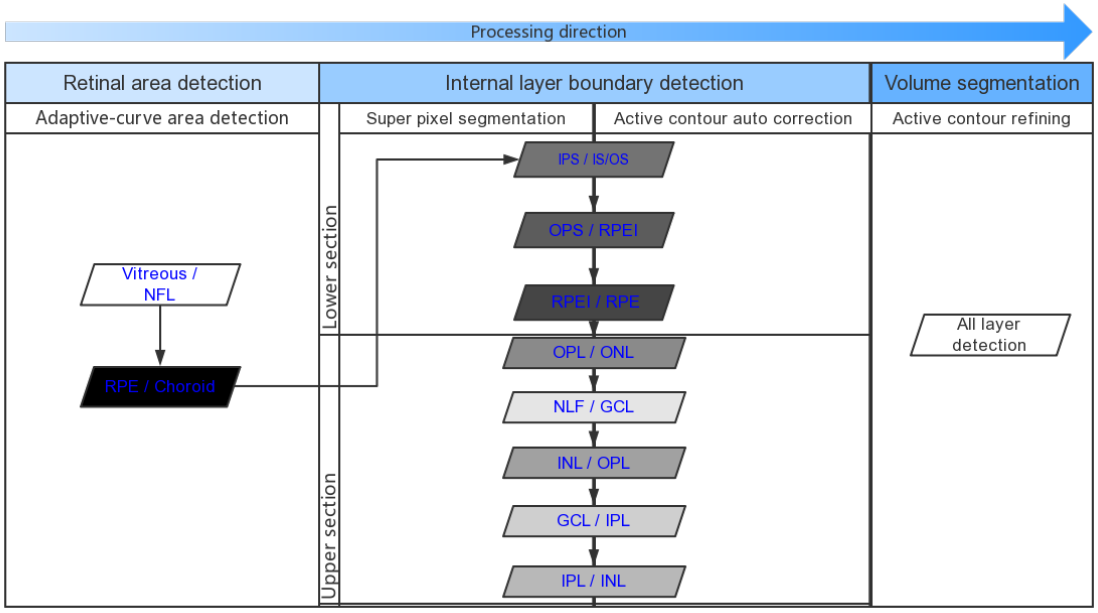

Figure 6. The sequence of 10 boundaries segmentation. The framework first detect the region edges with adaptive-curve detection method. Then three internal cell layers located a bottom is segmented from top. Finally, the remaining boundaries are segmented. With the segmentation results in B-scan, the surface of each layer in the 3D volume can be fitted by using active contour.

3.1 Segmentation Results for Vitreous/NFL Boundary

The detection of the vitreous/NFL boundary is usually done within several iterations of the adaptive-curve algorithm. In Figure 7 we show the boundary detection in both 3D volume and B-scan images selected from the volume. It is seen in the Figure 7 (A) that the 3D registration process enforces the continuity and smoothness of the surfaces between adjacent B-scans and the top surface, indicating the boundary between the vitreous and NFL. Figure 7 (B,C) shows the segmentation in a single B-scan, selected from the 3D volume. It is observed that the active contour ignores the perfectly linear stripe artifacts present in all B-scan images comprising our dataset.

3.2 Results of Segmenting a Single B-scan Image

The segmentation of 12 boundaries on a single B-scan image is shown in Figure 8. The B-scan image was directly segmented by the framework without any pre-denoising process. Due to the high resolution and limited speckle noise, the thin layers embedded at bottom are clearly presented and their boundaries are clearly preserved. The high intensity response of the fovea point is due to the focusing point of the system. The foveal region shown in Figure 8 (B) provides a closer look at the merging of layer boundaries at fovea. Here thin layer boundaries are preserved and segmented using our method. Figure 8 (C) shows the segmentation at left side of fovea where our method provides stable segmentation results in the upper layers which have lower contrast than the bottom layers.

3.3 Results for Segmentation of a 3D Volume

We also tested the boundary segmentation in the denoised 3D volume data. The data is generated from a different system which presents retinal tissue with a relatively low contrast. It is seen from Figure 9 that the noise was suppressed by a 3D mean filter. As a side-effect, the layer boundaries are also blurred. In this 3D volume, we segment 10 surfaces corresponding to layer boundaries. By segmenting the surface of each layer, we can further calculate the thickness of each cell layer, for instance, the NFL layer shown in the Figure 9 (C). In

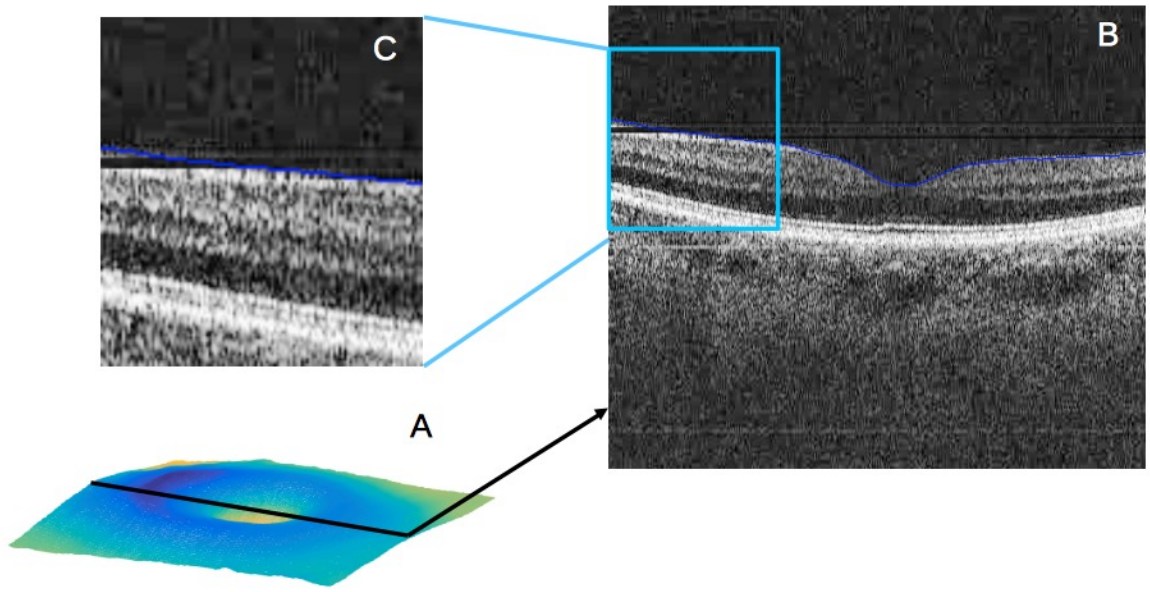

Figure 7. The segmentation results of the vitreous/NFL boundary. (A): The segmented boundary surface from the 3D volume. (B,c): The B-scan image selected from the black line in (A). It is seen that the surface can be well fitted when the stripe noise, which partially covers the image content, was replaced with zeros.

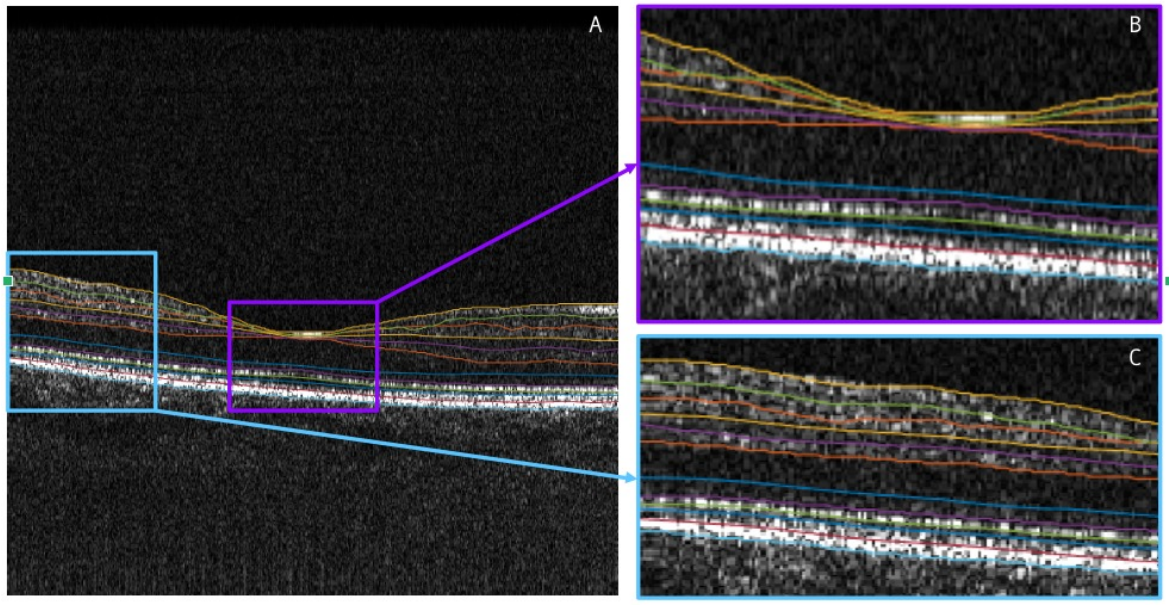

Figure 8. The segmentation result of 12 boundaries in the single B-scan. (A):The segmentation was process on the original OCT image without pre-denoising. (B,C): the zoomed view of (A).

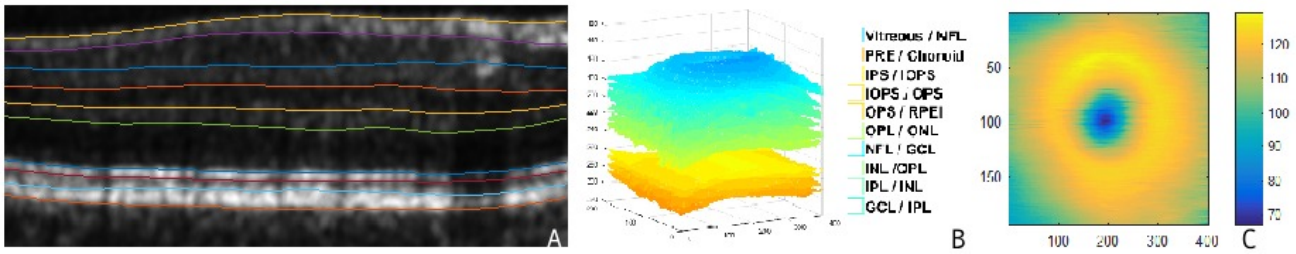

Figure 9. The segmentation result of 10 boundaries in the 3D volume. (A):The segmentation was process on the original OCT image without pre-denoising. (B): The surface model of segmented boundaries. (C): The thickness map of the NFL layer calculated from the volume segmentation.

Figure 9 (A), we see that the blood vessel in the upper layers produces a large reflection, resulting in a shadow underneath. By using superpixels and active contours, the boundary segmentation was not affected by the blood vessel. This indicates the robustness of our algorithm to the inconsistence of intensity of entire layer tissue.

4. CONCLUSION AND FUTUREWORK

In this paper, we proposed an boundary segmentation framework for retinal OCT images and volumes. The proposed adaptive-curve detection method searches the retinal region with boundary evolution. The SLIC superpixels, and the modified active contour, segment the remaining boundaries in a sequential order. The framework was tested on 3D OCT volumes which were generated with two different OCT systems. In the results, 10 and 12 boundaries were detected in separate datasets. Additionally, a 3D surface model and layer thickness map were also generated.

We have demonstrated that by combining superpixels and active contour methods, cell layers can be reliably segmented from low contrast B-scans containing strong speckle noise. In low contrast regions, the superpixels can group local pixels according to contrast in A-scans. Also, the active contour balances contour shape and gradient information to reduce the influence of blood vessels and their shadows.

Future work will include testing our approach using a large dataset from a different OCT system and a bench mark analysis with alternative methods, previously reported, methods. We will investigate the use of 3D supervoxels to improve computational efficiency. In addition, because our method is computed based on A-scans, it is amenable to a parallel implementation that utilizes GPU acceleration, thereby further reducing overall processing time.

REFERENCES

[1] Wojtkowski, M., Bajraszewski, T., Gorczyńska, I., Targowski, P., Kowalczyk, A., Wasilewski, W., and Radzewicz, C., "Ophthalmic imaging by spectral optical coherence tomography," *American journal of ophthalmology* **138**(3), 412–419 (2004).

[2] Browning, D. J., McOwen, M. D., Bowen, R. M., and Tisha, L. O., "Comparison of the clinical diagnosis of diabetic macular edema with diagnosis by optical coherence tomography," *Ophthalmology* **111**(4), 712–715 (2004).

[3] Schmitt, J. M., Xiang, S., and Yung, K. M., "Speckle in optical coherence tomography: an overview," SPIE (1999).

[4] DeBuc, D. C., "A review of algorithms for segmentation of retinal image data using optical coherence tomography," in [*Image Segmentation*], InTech (2011).

[5] Koozekanani, D., Boyer, K., and Roberts, C., "Retinal thickness measurements from optical coherence tomography using a markov boundary model," *IEEE transactions on medical imaging* **20**(9), 900–916 (2001).

[6] Ishikawa, H., Stein, D. M., Wollstein, G., Beaton, S., Fujimoto, J. G., and Schuman, J. S., "Macular segmentation with optical coherence tomography," *Investigative ophthalmology & visual science* **46**(6), 2012–2017 (2005).

[7] Shahidi, M., Wang, Z., and Zelkha, R., "Quantitative thickness measurement of retinal layers imaged by optical coherence tomography," *American journal of ophthalmology* **139**(6), 1056–1061 (2005).

[8] Chiu, S. J., Li, X. T., Nicholas, P., Toth, C. A., Izatt, J. A., and Farsiu, S., "Automatic segmentation of seven retinal layers in sdoct images congruent with expert manual segmentation," *Optics express* **18**(18), 19413–19428 (2010).

[9] Yang, Q., Reisman, C. A., Wang, Z., Fukuma, Y., Hangai, M., Yoshimura, N., Tomidokoro, A., Araie, M., Raza, A. S., Hood, D. C., et al., "Automated layer segmentation of macular oct images using dual-scale gradient information," *Optics express* **18**(20), 21293–21307 (2010).

[10] Kajić, V., Považay, B., Hermann, B., Hofer, B., Marshall, D., Rosin, P. L., and Drexler, W., "Robust segmentation of intraretinal layers in the normal human fovea using a novel statistical model based on texture and shape analysis," *Optics express* **18**(14), 14730–14744 (2010).

[11] Kajić, V., Esmaeelpour, M., Považay, B., Marshall, D., Rosin, P. L., and Drexler, W., "Automated choroidal segmentation of 1060 nm oct in healthy and pathologic eyes using a statistical model," *Biomedical optics express* **3**(1), 86–103 (2012).

[12] Kafieh, R., Rabbani, H., Abramoff, M. D., and Sonka, M., "Intra-retinal layer segmentation of 3d optical coherence tomography using coarse grained diffusion map," *Medical image analysis* **17**(8), 907–928 (2013).

[13] Tian, J., Varga, B., Somfai, G. M., Lee, W.-H., Smiddy, W. E., and DeBuc, D. C., "Real-time automatic segmentation of optical coherence tomography volume data of the macular region," *PloS one* **10**(8), e0133908 (2015).

[14] Vermeer, K., Van der Schoot, J., Lemij, H., and De Boer, J., "Automated segmentation by pixel classification of retinal layers in ophthalmic oct images," *Biomedical optics express* **2**(6), 1743–1756 (2011).

[15] Lang, A., Carass, A., Hauser, M., Sotirchos, E. S., Calabresi, P. A., Ying, H. S., and Prince, J. L., "Retinal layer segmentation of macular oct images using boundary classification," *Biomedical optics express* **4**(7), 1133–1152 (2013).

[16] Wang, M., Liu, X., Gao, Y., Ma, X., and Soomro, N. Q., "Superpixel segmentation: A benchmark," *Signal Processing: Image Communication* **56**, 28–39 (2017).

[17] Yushkevich, P. A., Piven, J., Hazlett, H. C., Smith, R. G., Ho, S., Gee, J. C., and Gerig, G., "User-guided 3d active contour segmentation of anatomical structures: significantly improved efficiency and reliability," *Neuroimage* **31**(3), 1116–1128 (2006).

[18] Achanta, R., Shaji, A., Smith, K., Lucchi, A., Fua, P., and Süsstrunk, S., "Slic superpixels compared to state-of-the-art superpixel methods," *IEEE transactions on pattern analysis and machine intelligence* **34**(11), 2274–2282 (2012).

[19] Bakoš, M., "Active contours and their utilization at image segmentation," in [*5th Slovakian-Hungarian Joint symposium on applied machine intelligence and informatics, Poprad, Slovakia*], (2007).